

Measurement of proton-proton elastic scattering at 6 GeV/c in polarized initial and final spin states*

M. Borghini

CERN, Geneva 23, Switzerland

W. de Boer,[†] R. C. Fernow, A. D. Krisch, H. E. Miettinen,[‡] T. A. Mulera,[§] J. B. Roberts[§]
and K. M. Terwilliger

Randall Laboratory of Physics, The University of Michigan, Ann Arbor, Michigan 48109

J. R. O'Fallon^{||}

Department of Physics, St Louis University, St. Louis, Missouri 63103

L. R. Ratner

Accelerator Research Facilities Division, Argonne National Laboratory, Argonne, Illinois 60439

(Received 11 July 1977)

The differential elastic p - p scattering cross section was measured at 6 GeV/c at the Argonne Zero Gradient Synchrotron in the range $P_{\perp}^2 = 0.60$ – 1.0 (GeV/c)² using a 65% polarized target and a 75% polarized proton beam of intensity 3×10^9 protons/pulse. The polarization of the recoil proton was simultaneously measured with a well calibrated carbon-target polarimeter. All three polarizations were measured perpendicular to the horizontal scattering plane. Our results indicate that P and T invariance are both obeyed to good precision even at our largest P_{\perp}^2 . Parity invariance implies that the eight single-flip transversity cross sections are zero, so our data gives the magnitudes of the eight remaining pure spin cross sections where all spins are measured. We find that the four double-flip transversity cross sections are nonzero.

I. INTRODUCTION

In recent years there has been a growing recognition that high-energy strong interactions have an important spin dependence. This began with the very successful experiments using polarized targets at Berkeley,¹ CERN,² and Argonne.³ The Zero Gradient Synchrotron (ZGS) polarized proton beam allows even more extensive and precise studies of this spin dependence, especially when used along with a polarized target. During the past few years, our group^{4,6} and the ANL-Northwestern group⁵ have studied proton-proton elastic scattering in polarized initial spin states. We found large differences between the two-spin cross sections (both initial spins measured), especially at large P_{\perp}^2 . By taking advantage of the beam spin being reversed on alternate pulses, we were able to measure the two-spin cross sections with a precision of about $\pm 0.3\%$. Such high precision allows a more detailed study of spin dependence than was previously possible.

We also measured⁶ the polarization of the recoil proton at $P_{\perp}^2 = 0.5$ (GeV/c)² and found some evidence for a nonzero double spin-flip transversity cross section. We have now improved our carbon-target recoil polarimeter by adding hodoscopes upstream, tightening its angular resolution, and calibrating it in the appropriate energy accelerated polarized proton beam. This improvement combined with the greater polarized-beam intensity has allowed us to measure the eight pure

three-spin cross sections out to $P_{\perp}^2 = 1.0$ (GeV/c)² with reasonable precision.

In the following section we discuss some general properties of spin parameters. We have found it convenient to discuss the results of our experiment in terms of pure spin cross sections. We describe this formalism together with the older Wolfenstein formalism and the relation between the two. Section III contains a description of the experimental apparatus and operating procedures including the polarized beam and target, the high-energy polarimeter, the elastic-event spectrometer, the recoil polarimeter, and its calibration. Section IV discusses our data analysis. Included here are calculations of cross sections and Wolfenstein parameters and discussion of errors. The final section gives our results in terms of pure spin cross sections and Wolfenstein parameters. This section also contains results for tests of parity and time-reversal invariance and a discussion of the significance of our measurements.

II. GENERAL PROPERTIES OF SPIN PARAMETERS

A. Pure spin cross sections

We studied proton-proton elastic scattering with the beam and target spins both oriented normal to the horizontal scattering plane. In addition, we simultaneously measured the polarization of the recoil particle along this same normal to the scattering plane

$$\hat{n} = \vec{k}_{in} \times \vec{k}_{out}. \quad (2.1)$$

In general, the p - p interaction is dependent on the spin state of each proton. We present the results of our experiment in terms of a set of cross sections for scattering in pure spin states. There are 16 of these pure four-spin cross sections corresponding to the 16 different possibilities for orienting four spin- $\frac{1}{2}$ particles. These cross sections will be denoted

$$d\sigma/dt(ij \rightarrow kl), \quad (2.2)$$

where the indices ($ij \rightarrow kl$) denote the spin orientation of the (beam, target \rightarrow scattered, recoil) particles. Each index may be either \uparrow or \downarrow , depending on whether the spin is parallel or antiparallel to \hat{n} . These 16 quantities are the pure spin transversity cross sections.

We measured the four two-spin cross sections denoted by $d\sigma/dt(ij)$, where both initial polarizations are measured but both final polarizations are unmeasured.

$$d\sigma/dt(ij) = \sum_{kl} d\sigma/dt(ij \rightarrow kl). \quad (2.3)$$

We obtained these with rather high precision since they do not require a measurement of recoil polarization. Rotational invariance and identical particle symmetry require that $d\sigma/dt(\uparrow\uparrow) = d\sigma/dt(\downarrow\downarrow)$.

The familiar elastic cross section with an unpolarized beam and an unpolarized target will be called the spin-average cross section $\langle d\sigma/dt \rangle$.

This is given by

$$\begin{aligned} \left\langle \frac{d\sigma}{dt} \right\rangle &= \frac{1}{4} \left(\frac{d\sigma}{dt}(\uparrow\uparrow) + \frac{d\sigma}{dt}(\uparrow\downarrow) + \frac{d\sigma}{dt}(\downarrow\uparrow) + \frac{d\sigma}{dt}(\downarrow\downarrow) \right) \\ &= \frac{1}{4} \sum_{ijkl} \frac{d\sigma}{dt}(ij \rightarrow kl). \end{aligned} \quad (2.4)$$

The factor $\frac{1}{4}$ arises from averaging over initial states and summing over final states.

Using the asymmetry measurements from the recoil polarimeter we could calculate the eight pure three-spin cross sections. Each of these cross sections is the sum of two of the pure four-spin cross sections

$$\frac{d\sigma}{dt}(ij \rightarrow 0l) = \frac{d\sigma}{dt}(ij \rightarrow \uparrow l) + \frac{d\sigma}{dt}(ij \rightarrow \downarrow l), \quad (2.5)$$

where the 0 indicates that the polarization of the scattered proton is unmeasured. The statistical accuracy of the three-spin cross sections is much worse than that of the two-spin cross sections since the recoil particle must be rescattered.

The 16 pure four-spin cross sections for the elastic scattering of identical spin- $\frac{1}{2}$ particles are not all independent observables. The laws of parity conservation (P), time-reversal invariance (T), identical-particle symmetry (X), and rotational invariance of space (R) reduce the number of in-

dependent complex amplitudes to five. Since one phase is arbitrary there are nine independent numbers. Our experiment measured the magnitudes of the five transversity amplitudes, but gave no information about the phases. Obtaining information about the phases will require experiments that measure components of the polarizations in the scattering plane. However, we are able to use the fact that our system is overconstrained to make tests of P and T invariance described in Sec. VB. The invariance properties of the pure spin cross sections are also discussed in that section.

B. Wolfenstein formalism

An alternative method of describing the results of polarization experiments uses the Wolfenstein parameters.⁷ For the case of p - p elastic scattering, Wolfenstein and Ashkin showed⁸ that the expectation values of final-state spin operators were related to expectation values of the initial-state spin operators thru the relation

$$4 \frac{d\sigma_f}{d\Omega} \langle S_\mu \rangle_f = \sum_\nu \langle S_\nu \rangle_i \text{Tr}(MS_\nu M^\dagger S_\mu), \quad (2.6)$$

where the S_μ are a set of 16 linearly independent spin operators and M is the 4×4 scattering matrix.

For the present case of a polarized beam and polarized target Eq. (2.6) leads to⁹

$$\frac{d\sigma}{dt} = \left\langle \frac{d\sigma}{dt} \right\rangle (1 + P_B A_B + P_T A_T + P_B P_T A_{nn}), \quad (2.7)$$

where $\langle d\sigma/dt \rangle$ is the spin-averaged cross section, P_B and P_T are the beam and target polarizations, A_B is the analyzing power averaged over the target polarization, A_T is the analyzing power averaged over the beam polarization, and A_{nn} gives the cross sectional dependence on the product of P_B and P_T . Rotational invariance and identical particle symmetry require that

$$A_B = A_T = A, \quad (2.8)$$

while T invariance demands that

$$A_{nn} = C_{nn}, \quad (2.9)$$

where C_{nn} is the correlation between the components of the final-state polarizations in the normal direction. Rewriting Eq. (2.7) we obtain

$$\frac{d\sigma}{dt} = \left\langle \frac{d\sigma}{dt} \right\rangle [1 + (P_B + P_T)A + P_B P_T C_{nn}]. \quad (2.10)$$

Equation (2.6) also leads to the recoil particles' polarization in the \hat{n} direction, P_R , through the relation⁹

$$P_R \frac{d\sigma}{dt} = \left\langle \frac{d\sigma}{dt} \right\rangle (P + P_B K_{nn} + P_T D_{nn} + P_B P_T C_{3n}), \quad (2.11)$$

where P is the polarization parameter, K_{mn} is one component of the beam-recoil spin-transfer tensor, D_{mn} is one component of the target-recoil depolarization tensor, and C_{3n} is one component of the tensor showing the correlation of the recoil particles' polarization in the \hat{n} direction with the product of the beam and target polarizations in the \hat{n} direction. Parity invariance requires that

$$P = C_{3n}, \quad (2.12)$$

while T invariance demands that

$$P = A. \quad (2.13)$$

Substituting into Eq. (2.11) we find that

$$P_R \frac{d\sigma}{dt} = \left\langle \frac{d\sigma}{dt} \right\rangle [(1 + P_B P_T)A + P_B K_{nn} + P_T D_{nn}]. \quad (2.14)$$

C. Relations between the formalisms

It is instructive to show the relations between the Wolfenstein parameters discussed in the preceding section and the pure spin cross sections introduced in Sec. II A. Let us define the pure-state cross-section ratios

$$\sigma(ij) = \frac{d\sigma/dt(ij)}{\langle d\sigma/dt \rangle} \quad (2.15)$$

and

$$\sigma(ij \rightarrow 0l) = \frac{d\sigma/dt(ij \rightarrow 0l)}{\langle d\sigma/dt \rangle}. \quad (2.16)$$

Then the analyzing power A_B is given by

$$4A_B = \sigma(\uparrow\uparrow) + \sigma(\uparrow\downarrow) - \sigma(\downarrow\uparrow) - \sigma(\downarrow\downarrow), \quad (2.17)$$

the analyzing power A_T by

$$4A_T = \sigma(\uparrow\uparrow) - \sigma(\uparrow\downarrow) + \sigma(\downarrow\uparrow) - \sigma(\downarrow\downarrow), \quad (2.18)$$

and the spin-spin correlation C_{nn} by

$$4C_{nn} = \sigma(\uparrow\uparrow) - \sigma(\uparrow\downarrow) - \sigma(\downarrow\uparrow) + \sigma(\downarrow\downarrow). \quad (2.19)$$

Written out in full and assuming all the symmetry principles, the asymmetry parameter A and the spin-spin correlation parameter C_{nn} are given in terms of the pure two-spin cross sections by

$$A = \frac{d\sigma/dt(\uparrow\uparrow) - d\sigma/dt(\uparrow\downarrow)}{4\langle d\sigma/dt \rangle}, \quad (2.20)$$

$$C_{nn} = \frac{d\sigma/dt(\uparrow\uparrow) + d\sigma/dt(\uparrow\downarrow) - 2d\sigma/dt(\downarrow\uparrow)}{4\langle d\sigma/dt \rangle}.$$

For the second set of Wolfenstein parameters, Eq. (2.11), the polarization P is given by

$$4P = \sum_{ij} [\sigma(ij \rightarrow 0\uparrow) - \sigma(ij \rightarrow 0\downarrow)], \quad (2.21)$$

D_{nn} measures how the recoil polarization correlates with the target polarization,

$$4D_{nn} = \sum_{ij} [\sigma(ij \rightarrow 0j) - \sigma(ij \rightarrow 0, -j)], \quad (2.22)$$

K_{mn} measures how the recoil polarization correlates with the beam polarization,

$$4K_{nn} = \sum_{ij} [\sigma(ij \rightarrow 0i) - \sigma(ij \rightarrow 0, -i)], \quad (2.23)$$

and C_{3n} measures how the recoil polarization correlates with the product of beam and target polarizations,

$$4C_{3n} = \sum_{ij} [\sigma(ij \rightarrow 0, i \cdot j) - \sigma(ij \rightarrow 0, -i \cdot j)]. \quad (2.24)$$

III. EXPERIMENTAL APPARATUS AND PROCEDURES

A. Polarized beam

The experiment was performed using the Argonne ZGS polarized proton beam. This is described in detail in Khoe *et al.*,¹⁰ and we will only briefly review its operation.

The polarized protons start in a polarized-ion source which originally gave 8 μ A of 20-keV protons with a polarization of (70 \pm 5)%. This source was placed in the new pre-accelerator II dome where a Cockcroft-Walton column accelerates the protons to 750 keV. The protons are then fed into the main linear-accelerator (LINAC) line by a switching magnet and accelerated to 50 MeV. The polarization at 50 MeV is measured using a polarimeter which continuously monitors the left-right asymmetry in p -carbon elastic scattering at 55 $^\circ$ in the lab. Utilizing previous p -C results¹¹ we determined that the analyzing power of our 50-MeV polarimeter was (88 \pm 5)%. There is no measurable reduction of the beam polarization in the LINAC. The 50-MeV beam is injected into the ZGS, accelerated, and then extracted to the high-energy polarimeter described below.

The main problems in accelerating polarized protons in a synchrotron are "depolarizing resonances."¹² These occur when the Larmor precessional frequency becomes equal to the frequency with which the protons see horizontal magnetic field components. These perturbations can add coherently and rapidly depolarize the beam. The precessional frequency and the frequency of perturbations due to vertical betatron oscillations are

$$\omega_p = \left(\frac{g}{2} - 1\right)\gamma \frac{eB_0}{m}, \quad \omega_k = (k \pm \nu) \frac{eB_0}{m}. \quad (3.1)$$

The resonance condition which occurs when they are equal is

$$(g/2 - 1)\gamma = k \pm \nu, \quad (3.2)$$

where ν is the number of betatron oscillations per turn around the ZGS (~ 0.80), and k , an integer, is the harmonic number of the fields that perturb the protons (8 and 16 are the strongest). The resonances were jumped using two pulsed quadrupoles¹³ installed in the ZGS. By pulsing these in 20 μ sec, ν was rapidly changed and the beam passed through each resonance in a few turns before coherent depolarization could occur. The timing and strength of these pulses were tuned by maximizing the polarization measured in the high-energy polarimeter.

The 6-GeV/c extracted-polarized-beam intensity was about 3×10^9 protons per pulse, with one pulse every 2.5 sec. The accelerated intensity reached 6×10^9 /pulse, and the average beam polarization was $P_B = (75 \pm 4)\%$ for most data runs. These increases came from modifications in the polarized source, where Parker *et al.*¹⁴ took advantage of the pulsed nature of the ZGS to obtain pulses of 50 μ A at 20 keV, and from improving the resonant extraction efficiency of the ZGS to more than 50%.

Another important improvement was to flip the beam spin direction on alternate pulses by changing the rf frequency in the source.¹⁴ This new mode operated very reliably and made it possible to decrease biases between beam spin up and down runs. This feature allowed very-high-precision measurements of the beam spin dependence.

B. Polarized target

The polarized beam was scattered from the Michigan-Argonne PPT-V polarized proton target. This target is a close copy of a CERN target whose operation is discussed in Ref. 15. The details of PPT-V are given in Ref. 16, and we will only briefly describe its operation.

The target consists of frozen beads of propane-diol, $C_3H_8O_2$, doped with Cr paramagnetic complexes. The beads are 1–2 mm in diameter and are contained in a 4.1-cm-long by 2.9-cm-diameter cavity. The average density of hydrogen protons in the PPT is 0.073 ± 0.005 g/cm.³ The target is maintained at a temperature of 0.5 °K in a magnetic field of 25 kG. The free (hydrogen) protons of the target have spin-spin interactions with the highly polarized electrons of the Chromium-V complexes. These protons are given a comparably high polarization by applying microwave power with a frequency close to 70 GHz, obtained from a carcinotron tube. The direction of the target polarization can be reversed in 10–20 min by changing this frequency by a few hundred MHz.

The proton polarization was measured by using a nuclear-magnetic-resonance (NMR) system, operating at a frequency $f = 107$ MHz, with signal

averaging. The NMR system was calibrated against the calculable thermal-equilibrium polarization

$$P_{TE} = \frac{hf}{2kT}, \quad (3.3)$$

where h and k are the Planck and Boltzmann constants, respectively. This was measured during calibration runs with the microwaves off.

We installed two independent NMR coils in the PPT to monitor the spatial variation in P_T due to radiation damage from the high polarized beam intensity. Both coils were coaxial with the beam. One was a straight wire, while the other was a 15-mm-diameter helix. The two measured P_T values differed by less than 3%. This showed that the polarization was fairly uniform within the part of the PPT where most of the beam passed. The P_T measurements from the two coils were averaged. The target polarization has been as high as 85%, but the radiation damage to the target beads reduced the average P_T to just above 65%. Maintaining this average value required annealing the target every two days to remove some of the radiation damage and occasionally changing the target material.

C. High-energy polarimeter

The high-energy polarimeter shown in Fig. 1 is similar to that used in our earlier measurements.^{4,6,10} The beam polarization P_B is obtained by simultaneously measuring p - p elastic scattering to the left ($L = L_1 L_2 L_3 L_4 L_5 L_6$) and to the right ($R = R_1 R_2 R_3 R_4 R_5 R_6$). P_B is given by

$$P_B = \frac{1}{A} \left(\frac{L - R}{L + R} \right). \quad (3.4)$$

The polarimeter was operated at 6 GeV/c and $P_{\perp}^2 = 0.5$ (GeV/c)², where the asymmetry parameter for p - p elastic scattering is $A = 0.100 \pm 0.006$. This value was obtained by averaging our previous results with the data of other experiments.^{4,6}

The polarimeter consists of two double-arm spectrometers, each containing magnets and scintillation counters, and measures proton-proton elastic scattering from a liquid-hydrogen target. One measures the scattering of the forward particle to the left, while the other measures the scattering to the right. They both run simultaneously and continuously and are as identical as possible. The solid angle is defined by the counters L_3 and R_3 which are 15 cm \times 13 cm at ~ 20 m from the target giving $\Delta\Omega_{lab} \approx 50$ μ sr. The momentum bite defined by L_3 and R_3 is $\Delta P/P \approx \pm 6\%$. The overmatched counters L_6 and R_6 detected the recoil protons. Measuring both scattered particles gave a very

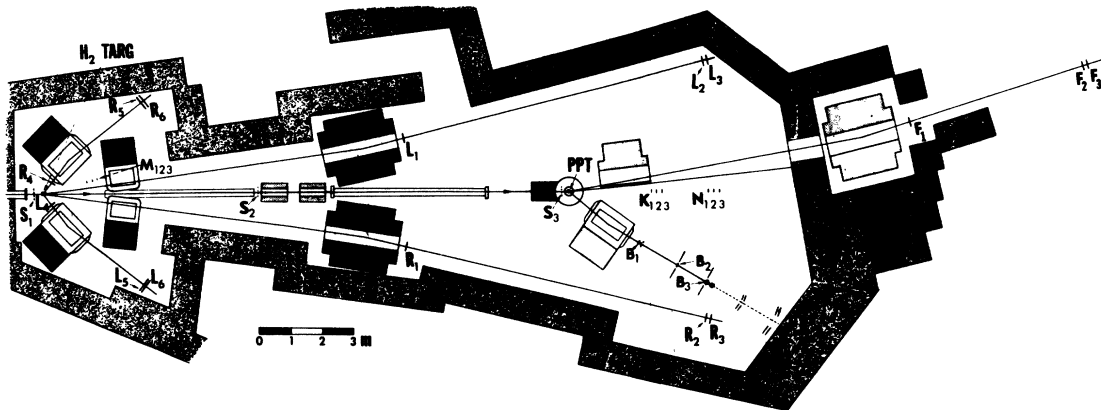


FIG. 1. Layout of the experiment. The polarized beam passes through the H_2 target, and its polarization is measured by comparing the number of elastic events seen in the L and R spectrometers of the polarimeter. The beam then scatters in the polarized proton target and the elastic events are counted by the FB spectrometer. The M , N , and K counters are monitors. The B polarimeter measures the spin of the recoil proton by measuring p -carbon scattering to the left and to the right.

clean elastic signal. The intensity of the beam incident on the target was measured with a three-counter telescope, denoted M . Target-empty runs and magnet curves showed that the background was 2% or less as shown in Fig. 2.

The polarimeter contained steering magnets so that at any incident momentum we could choose a P_{\perp}^2 value where the asymmetry parameter was measured and large. The six magnets were operated as three pairs of identical magnets. Each pair was run in series on one power supply so the

currents were identical. The central fields were measured and agreed to within 0.2% within each pair.

The main systematic asymmetry apparently comes from misalignments of the incident beam. The beam direction and position were continuously monitored using three segmented-wire ion chambers (S_1, S_2, S_3) with 2-mm wire spacing. Systematic errors in P_B were minimized by averaging the measurements of the two spectrometers and by flipping the beam spin between the up and down states on alternate pulses, and are estimated to be less than 1%. The value of P_B was monitored by the 50-MeV polarimeter and was independent of polarization direction within $\sim 1\%$. The extracted beam polarizations for spin up and spin down were determined from the average polarization obtained from the high-energy polarimeter corrected for the polarization differences observed at 50 MeV.

D. Elastic-event detector

The downstream double-arm spectrometer measured the elastic cross section for scattering the polarized proton beam to the left from the polarized target (PPT). Each arm contains magnets and scintillation counters $F = F_1 F_2 F_3$ and $B = B_1 B_2 B_3$ which respectively detect the forward (scattered) and backward (recoil) protons; a coincidence between the two arms is labeled FB . The nominally defining F_3 counter, which was about $15\text{ cm} \times 13\text{ cm}$ (horizontal \times vertical) and was about 18.4 m from the PPT, subtended a solid angle of $\Delta\Omega_{\text{lab}} \sim 5.7\ \mu\text{sr}$, and a momentum bite of $\Delta P/P \sim \pm 7\%$. The B_3 counter, which was about $5\text{ cm} \times 20\text{ cm}$ and was about 5.5 m from the PPT, subtended a solid angle which

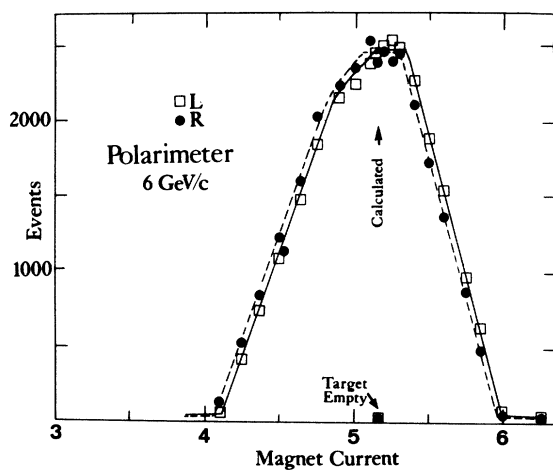


FIG. 2. Event rate in the L and R sides of the high-energy polarimeter plotted against the recoil magnet current (in arbitrary units). Notice the slight shift between the L and R sides, indicating that the incident beam is slightly misaligned. A target-empty run is also shown.

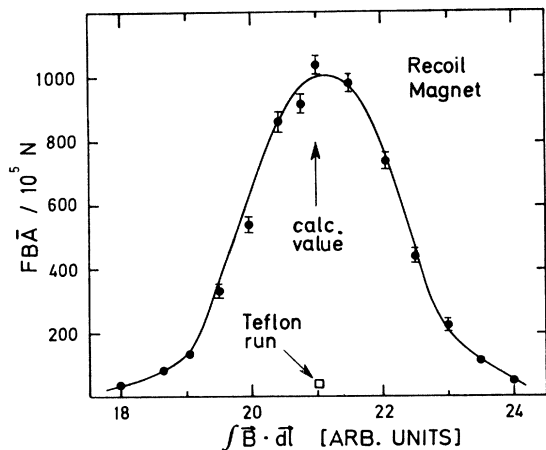


FIG. 3. Event rate in the FB spectrometer plotted against the recoil magnet $\int \vec{B} \cdot d\vec{l}$ for elastic scattering from the PPT at 6 GeV/c and $P_{\perp}^2 = 0.6$ (GeV/c) 2 . The Teflon run is also shown. The \bar{A} in the event rate $FB\bar{A}$ refers to an anticoincidence (shown in Fig. 5) used to reduce background.

was typically almost equal to the “matched” solid angle of F_3

$$\Delta\Omega_{\text{match}} \equiv \left(\frac{J_{\text{forward}}}{J_{\text{recoil}}} \right) \Delta\Omega_{F_3}, \quad (3.5)$$

where each Jacobian J relates the corresponding lab solid angle to the c.m. solid angle.

This equality results in a lack of adequate “overmatching” and a resulting loss of events which made it impossible to know the true effective solid angle of the FB spectrometer, especially at $P_{\perp}^2 = 0.6$ (GeV/c) 2 . Inscattering is automatically equal to outscattering in a single-arm experiment. Making them equal in a double-arm experiment requires defining $\Delta\Omega$ with one arm and making the other arm adequately overmatched to ensure that each mate particle is counted in spite of the beam’s angular divergence and spot size, multiple Coulomb scattering in the PPT and early counters, and other similar effects. We decided to sacrifice an exact knowledge of $\Delta\Omega$ to reduce the number of accidental and other background events to a very low level. Background events are especially serious in PPT experiments because $\sim 90\%$ of the nucleons in propanediol are not free protons. Moreover, only $\sim 1\%$ of the recoil protons from FB events scattered from the carbon target and triggered the B polarimeter.

Therefore, we sacrificed absolutely normalized cross sections to obtain an unusually clean elastic signal. Instead, we measured the ratios $\sigma(ij)$ and $\sigma(ij \rightarrow 0l)$ given in Eqs. (2.15) and (2.16). We then normalized the pure spin cross sections using measurements of $\langle d\sigma/dt \rangle$ made with unpolarized tar-

gets and beams.¹⁷

The FB accidentals were only about $\frac{1}{4}\%$ of FB . They were continuously monitored and subtracted. We measured inelastic events and the background from the nonhydrogen nucleons in the PPT by replacing the propanediol beads with Teflon beads which contain no hydrogen protons. The Teflon event rate was $(3.9 \pm 0.2)\%$ of the normal event rate both at $P_{\perp}^2 = 0.6$ and 1.0 (GeV/c) 2 . We also ran magnet curves, where we measured the FB rate while varying $\int \vec{B} \cdot d\vec{l}$ in the recoil magnet. As shown in Fig. 3 the event rate dropped by a factor of 30 when $\int \vec{B} \cdot d\vec{l}$ was detuned by 20% from the calculated value. This gave further evidence for a clean elastic signal from the free protons in the PPT. The almost nonexistence of a flat top is an unfortunate consequence of the lack of overmatching.

Quadrupoles were installed between the hydrogen target and the PPT to reduce the beam size at the PPT to about 18 mm full width at half-maximum (FWHM). The beam was kept centered to about 2 mm using the segmented-wire ion chambers. This reduced possible systematic errors in the cross sections and Wolfenstein parameters due to beam motion in the 2.9-cm-diameter target. These systematic errors were further reduced by flipping the direction of the beam spin on alternate pulses and the target spin every 12 h.

The relative number of polarized protons incident on the PPT was measured by two monitors located downstream of the target. They consisted of independent three-counter telescopes, denoted N and K . These were placed above and below the median plane in a vertical plane containing the beam and target so that their counting rates would not depend on the direction of the beam or target polarization.

We also ran beam steering curves by changing

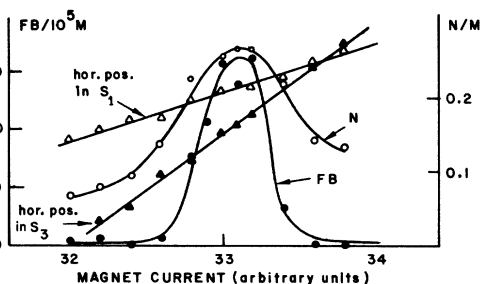


FIG. 4. Beam steering curve. The ratios FB/M and N/M are both plotted against the current in a steering magnet near the H_2 target. The FB spectrometer and the N monitor both look at the PPT, while the M monitor looks at the H_2 target. Also plotted are the beam positions at the various SWIC’s shown in Fig. 1.

the $\int \vec{B} \cdot d\vec{l}$ in two of the bending magnets in the beam transport line just upstream of the H_2 target. This minimized the asymmetry in the high-energy polarimeter, and ensured that the beam hit the center of the PPT. Such a curve is shown in Fig. 4 where we have plotted the FB/M and N/M ratios, as well as the beam position at various segmented-wire ion chambers (SWIC). The maximum in the FB/M rate was used to determine the appropriate SWIC positions for data runs.

E. Recoil polarimeter

The spin of the recoil proton was measured by the B polarimeter shown in Fig. 1 and in more detail in Fig. 5. This detects the recoil protons which scatter from a 13-cm-long carbon target into four-fold scintillation counter telescopes subtending the range $\theta_{\text{lab}} = 7^\circ - 11^\circ$. The defining counters B_{L4} and B_{R4} were about 17 cm \times 40 cm (horizontal \times vertical) and about 2.3 m from the C target. We measured the asymmetry A_m in p -carbon scattering to the left ($B_L = FB\bar{A} \cdot B_{L1} B_{L2} B_{L3} B_{L4}$) and to the right ($B_R = FB\bar{A} \cdot B_{R1} B_{R2} B_{R3} B_{R4}$)

$$A_m = \frac{B_L - B_R}{B_L + B_R}, \quad (3.6)$$

where $FB\bar{A}$ is the elastic-event trigger. We then obtained the recoil proton's polarization P_R from the relation

$$P_R = \frac{A_m - D}{A_C - A_m E}, \quad (3.7)$$

where A_C is essentially the p -C analyzing power

or asymmetry parameter for the polarimeter. D and E reflect biases of the polarimeter due to counter inefficiency, surveying or construction errors, and the angular and positional variation of the recoil protons heading into the carbon target. When D and E are zero Eq. (3.7) reduces to the simple Eq. (3.4) used for the high-energy polarimeter where these biases could be removed. However, the protons heading into the B polarimeter were not a well-collimated beam, but were spread over an angular range which was large enough to give an adequate event rate [$\Delta P_{\perp}^2 \sim 0.04$ (GeV/c) 2]. Thus, D and E were not negligible, and they had to be known along with A_C for each recoil-proton momentum and for each possible angle and position of a recoil proton heading into the polarimeter.

We, therefore, installed two five-channel hodoscopes ($H_1 H_{12} H_2 H_{23} H_3$ and $H_4 H_{45} H_5 H_{56} H_6$) just upstream of the carbon target. These monitored the angle and position of each recoil proton that triggered an $FB\bar{A}$ coincidence by assigning each event to one channel of a 5×5 matrix. This information was recorded using a CAMAC discriminator-coincidence register (DCR) coupled to a PDP11/10 computer. The DCR also recorded if B_L or B_R had fired.

To reduce the number of accidental and inelastic events in B_L and B_R , we installed the anticounters A_1 or A_2 or A_3 or $A_4 = A$ shown in Fig. 5. We also packed lead between the B -polarimeter counters and the PPT and set the angle of bend in the recoil magnet to 20° . The Teflon runs gave a $B_L + B_R$ rate of $(3.9 \pm 0.7)\%$ of the normal rate at both P_{\perp}^2

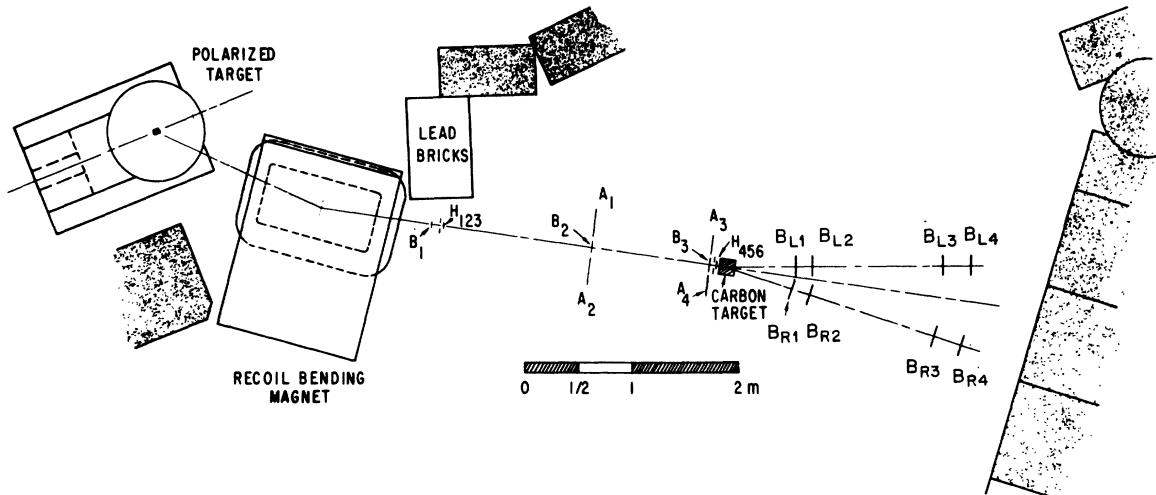


FIG. 5. Layout of the recoil (B) arm and the B polarimeter. The recoil proton is momentum analyzed by the recoil magnet and then detected by the $B_1 B_2 B_3$ counters. The H_{123} and H_{456} hodoscopes monitor its angle and position prior to its scattering from the carbon target, while the B_L and B_R telescopes detect the p -C scattering to the left and the right. The A counters reduce background.

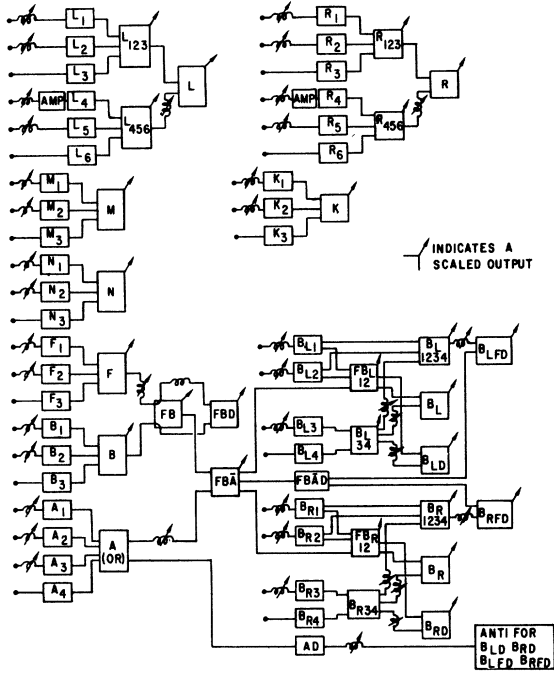


FIG. 6. The electronics block diagram showing the logic for detecting events and monitoring accidentals.

$= 0.6$ and 1.0 (GeV/c)²; and within statistics B_L and B_R were equal. We, therefore, made a 3.9% subtraction from both B_L and B_R at all three P_{\perp}^2 values. This had the effect of increasing the recoil polarization P_R and all three-spin parameters a relative 4%; the largest absolute effect was on D_{nn} which was increased about 3%. The $\pm 0.7\%$ uncertainty in this inelastic correction gave an uncertainty in the three-spin cross sections of about $\pm \frac{1}{2}\%$ of the spin-average cross section.

Several types of accidentals were monitored as indicated in Fig. 6. The B_{LD} circuit looked at accidentals between $FB\bar{A} \cdot B_{L12}$ and B_{L34} , while B_{LFD} monitored accidentals between $FB\bar{A}$ and B_{L1234} . Typically $(B_{LD} + B_{RD})/(B_L + B_R)$ was $(2.7 \pm 0.2)\%$, while $(B_{LFD} + B_{RFD})/(B_L + B_R)$ was $(0.3 \pm 0.1)\%$. Both were monitored continuously and subtracted from B_L and B_R .

F. Calibration runs

We calibrated the hodoscope-polarimeter system by physically moving it into the main ZGS polarized beam and taking calibration runs with the polarized beam accelerated to the appropriate recoil-proton momentum for each P_{\perp}^2 value: 870 MeV/c for $P_{\perp}^2 = 0.6$, 1050 MeV/c for $P_{\perp}^2 = 0.8$, and 1220 MeV/c for $P_{\perp}^2 = 1.0$ (GeV/c)². The polarimeter axis and the axis of the hodoscopes should be closely aligned for both the calibration and data runs. We surveyed

them very carefully to a precision of $\pm \frac{1}{4}$ mr, for both runs, keeping misalignment errors in the three spin cross sections below $\pm 1\%$.

These calibration runs required a good knowledge of the beam polarization, P_B . As discussed earlier, we measured P_B just before acceleration with the 50-MeV polarimeter, which we determined to have an analyzing power of $(88 \pm 5)\%$ for p -C scattering at $\theta_{\text{lab}} = 55^\circ$ and 50-MeV kinetic energy. There should be no significant depolarization during acceleration up to the first weak intrinsic depolarizing resonance¹⁰ at 1.39 GeV/c. We believe that our assumption $P_B = P_B(50 \text{ MeV})$ is good to 2% in this region.

The calibration runs gave A_C^n , D^n , and E^n for each of the 25 hodoscope channels with about 1% precision. For the central channel H_2H_5 , $D^{2,5}$ and $E^{2,5}$ were very close to zero (< 0.01), while for the most extreme channels D and E were quite large; for example, $D^{1,6} \approx -0.35$ and $E^{1,6} \approx -0.12$.

The behavior of A_C is interesting nuclear physics, since it is the asymmetry parameter for p -C scattering at $\theta_{\text{lab}} = 9 \pm 2^\circ$. The events are probably mostly elastic, although we made no specific elastic cut. We plot A_C in Fig. 7 against the average kinetic energy halfway through the 13-cm carbon target. The errors shown include the normalization error coming from the P_B measurement. The statistical error was typically less than $\frac{1}{2}\%$. Notice the surprisingly large value of $A_C = 59\%$ at about 280 MeV.¹⁸ The values of A_C obtained from this calibration and used in the experiment were: 59.2% for $P_{\perp}^2 = 0.6$, 44.6% for $P_{\perp}^2 = 0.8$, and 31.6% for $P_{\perp}^2 = 1.0$ (GeV/c)².

The fraction of the $FB\bar{A}$ events that were scattered and analyzed in the recoil polarimeter was

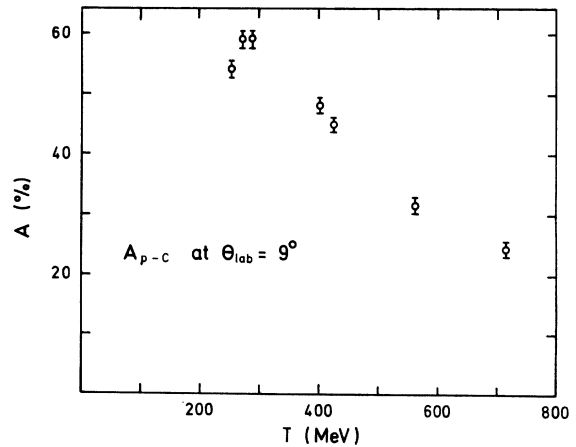


FIG. 7. Plot of the analyzing power for p -C scattering at $9^\circ \pm 2^\circ$ in the lab against the proton kinetic energy. The p -C events are mostly elastic.

TABLE I. Summary of polarizations and events. The errors are statistical.

P_{\perp}^2 [(GeV/c) ²]	0.5 ^a	0.6	0.8	1.0
P_B^+	0.63	0.664	0.734	0.715
P_B^-	0.64	0.666	0.748	0.717
P_T^+	0.77	0.604	0.662	0.669
P_T^-	0.70	0.696	0.619	0.679
$P_R(\uparrow\uparrow)$	0.82 ± 0.06	0.632 ± 0.035	0.615 ± 0.047	0.574 ± 0.057
$P_R(\uparrow\downarrow)$	-0.38 ± 0.08	-0.552 ± 0.048	-0.472 ± 0.047	-0.473 ± 0.057
$P_R(\downarrow\uparrow)$	0.64 ± 0.07	0.465 ± 0.039	0.527 ± 0.054	0.574 ± 0.066
$P_R(\downarrow\downarrow)$	-0.45 ± 0.09	-0.572 ± 0.049	-0.486 ± 0.048	-0.458 ± 0.062
$FB\bar{A}$	0.23 × 10 ⁶	1.00 × 10 ⁶	1.07 × 10 ⁶	1.23 × 10 ⁶
$B_L + B_R$	0.27 × 10 ⁴	0.73 × 10 ⁴	0.91 × 10 ⁴	1.20 × 10 ⁴

^a The $P_{\perp}^2 = 0.5$ (GeV/c)² data are from Ref. 6.

also fairly large for a rescattering experiment, typically

$$\frac{B_L + B_R}{FB\bar{A}} \cong 0.8\% . \quad (3.8)$$

At each energy this fraction was observed to be the same in the data runs and calibration runs to ± 5% (of the 0.8%) adding confidence that there was no serious additional background contamination in the data runs.

G. Data runs

As indicated earlier, the experimental runs were at a proton beam momentum of 6 GeV/c. We obtained approximately 10⁶ elastic $FB\bar{A}$ events and approximately 10⁴ recoil polarimeter analyzed events at each of three values of transverse momentum: $P_{\perp}^2 = 0.6, 0.8, \text{ and } 1.0$ (GeV/c)². The actual values are given in Table I, along with the average beam and target polarizations.

IV. DATA ANALYSIS

A. Two-spin cross sections

We obtained for each of the four initial spin states three quantities: the beam polarization $P_B(ij)$, the target polarization $P_T(ij)$, and a normalized event rate

$$N(ij) = \frac{FB\bar{A}(ij)}{I_0(ij)} . \quad (4.1)$$

For each run $FB\bar{A}(ij)$ is the measured number of elastic events, while $I_0(ij)$ is proportional to the number of incident protons, monitored by the M , N , and K monitors. These monitors were calibrated during aluminum-foil irradiation runs with

a 7% normalization uncertainty; however, our analyses did not use our absolute normalization.

The conventional way of obtaining A and C_m from the measured $N(ij)$ is given in equations 4 and 5 of Ref. 6, which can be directly derived from Eq. (2.10). This method assumes a stable beam-target configuration and is subject to systematic errors due to beam position variations between runs. As indicated before, we improved the precision by taking advantage of the beam spin being flipped on alternate pulses to average over some of these biases. However, the target polarization could only be reversed a couple of times each day, and significant effects of beam drift were observed on our A_T measurements. The analysis procedure employed, which is presented in the following discussion, essentially eliminates the dependence of A and C_m on beam motion on the target. This procedure, however, precludes making the test $A_B = A_T$, Eq. (2.8), since it is assumed in the analysis.

The four $N(ij)$ are related to A and C_m through Eq. (2.10):

$$\begin{aligned} N(\uparrow\uparrow) &= N_{\uparrow} \{ 1 + A [|P_B(\uparrow\uparrow)| + |P_T(\uparrow\uparrow)|] \\ &\quad + C_m |P_B(\uparrow\uparrow)| |P_T(\uparrow\uparrow)| \} , \\ N(\uparrow\downarrow) &= N_{\uparrow} \{ 1 + A [|P_B(\uparrow\downarrow)| - |P_T(\uparrow\downarrow)|] \\ &\quad - C_m |P_B(\uparrow\downarrow)| |P_T(\uparrow\downarrow)| \} , \\ N(\downarrow\uparrow) &= N_{\downarrow} \{ 1 + A [-|P_B(\downarrow\uparrow)| + |P_T(\downarrow\uparrow)|] \\ &\quad - C_m |P_B(\downarrow\uparrow)| |P_T(\downarrow\uparrow)| \} , \\ N(\downarrow\downarrow) &= N_{\downarrow} \{ 1 - A [|P_B(\downarrow\downarrow)| + |P_T(\downarrow\downarrow)|] \\ &\quad + C_m |P_B(\downarrow\downarrow)| |P_T(\downarrow\downarrow)| \} , \end{aligned} \quad (4.2)$$

where N_{\uparrow} is a normalization factor for the target-up runs and N_{\downarrow} is the equivalent factor for target-

TABLE II. Pure spin cross sections. Absolute cross sections are given in $\text{mb}/(\text{GeV}/c)^2$. The errors are statistical. The σ are cross-section ratios, defined in Eqs. (2.15) and (2.16).

$P_{\perp}^2 [(\text{GeV}/c)^2]$	0.5 ^a	0.6	0.8	1.0
$\sigma(\uparrow\uparrow\rightarrow 0\uparrow)$	1.31 ± 0.08	1.23 ± 0.04	1.15 ± 0.05	1.17 ± 0.06
$\sigma(\uparrow\uparrow\rightarrow 0\downarrow)$	-0.01 ± 0.08	0.06 ± 0.04	0.11 ± 0.05	0.18 ± 0.06
$\sigma(\uparrow\downarrow\rightarrow 0\uparrow)$	0.15 ± 0.08	0.05 ± 0.04	0.03 ± 0.05	0.11 ± 0.06
$\sigma(\uparrow\downarrow\rightarrow 0\downarrow)$	0.75 ± 0.08	0.84 ± 0.04	0.89 ± 0.05	0.83 ± 0.06
$\sigma(\downarrow\uparrow\rightarrow 0\uparrow)$	0.80 ± 0.08	0.77 ± 0.04	0.81 ± 0.05	0.83 ± 0.06
$\sigma(\downarrow\uparrow\rightarrow 0\downarrow)$	0.11 ± 0.08	0.12 ± 0.04	0.11 ± 0.05	0.11 ± 0.06
$\sigma(\downarrow\downarrow\rightarrow 0\uparrow)$	0.15 ± 0.08	0.07 ± 0.04	0.09 ± 0.05	0.07 ± 0.06
$\sigma(\downarrow\downarrow\rightarrow 0\downarrow)$	0.73 ± 0.08	0.86 ± 0.04	0.81 ± 0.05	0.69 ± 0.06
$\sigma(\uparrow\uparrow)$	1.295 ± 0.006	1.289 ± 0.006	1.264 ± 0.005	1.345 ± 0.005
$\sigma(\uparrow\downarrow)$	0.905 ± 0.004	0.893 ± 0.004	0.920 ± 0.004	0.943 ± 0.004
$\sigma(\downarrow\uparrow)$	0.895 ± 0.006	0.925 ± 0.006	0.896 ± 0.005	0.769 ± 0.006
$\sigma(\uparrow\uparrow\rightarrow\uparrow\uparrow)$	1.23 ± 0.08	1.23 ± 0.04	1.16 ± 0.05	1.23 ± 0.06
$\sigma(\uparrow\uparrow\rightarrow\uparrow\downarrow)$	0.07 ± 0.08	0.07 ± 0.04	0.10 ± 0.05	0.13 ± 0.06
$\sigma(\uparrow\uparrow\rightarrow\downarrow\uparrow)$	0.78 ± 0.08	0.81 ± 0.04	0.85 ± 0.05	0.83 ± 0.06
$\sigma(\uparrow\uparrow\rightarrow\downarrow\downarrow)$	0.13 ± 0.08	0.09 ± 0.04	0.07 ± 0.05	0.11 ± 0.06
$\sigma(\downarrow\uparrow\rightarrow\uparrow\uparrow)$	0.81 ± 0.08	0.87 ± 0.04	0.80 ± 0.05	0.64 ± 0.06
$\langle d\sigma/dt \rangle$	2.25	1.17	0.365	0.167
$d\sigma/dt (\uparrow\uparrow\rightarrow\uparrow\uparrow)$	2.77 ± 0.18	1.44 ± 0.05	0.423 ± 0.018	0.205 ± 0.010
$d\sigma/dt (\uparrow\uparrow\rightarrow\uparrow\downarrow)$	0.16 ± 0.18	0.08 ± 0.05	0.037 ± 0.018	0.021 ± 0.010
$d\sigma/dt (\uparrow\uparrow\rightarrow\downarrow\uparrow)$	1.76 ± 0.18	0.95 ± 0.05	0.310 ± 0.018	0.139 ± 0.010
$d\sigma/dt (\uparrow\uparrow\rightarrow\downarrow\downarrow)$	0.29 ± 0.18	0.11 ± 0.05	0.026 ± 0.018	0.018 ± 0.010
$d\sigma/dt (\downarrow\uparrow\rightarrow\uparrow\uparrow)$	1.82 ± 0.18	1.02 ± 0.05	0.292 ± 0.018	0.107 ± 0.010
ϵ_P	-0.05 ± 0.10	0.07 ± 0.05	0.08 ± 0.06	0.00 ± 0.08
ϵ_T	-0.16 ± 0.10	-0.01 ± 0.05	0.02 ± 0.06	0.11 ± 0.08

^a The $P_{\perp}^2=0.5 (\text{GeV}/c)^2$ data are from Ref. 6; the errors there include an assumed 10% uncertainty in the analyzing power A_C .

down runs. These equations assume rotational invariance and identical-particle symmetry. As indicated above, the N_{\uparrow} and N_{\downarrow} may be unequal because of beam motion or possible changes in counter efficiency between the target \uparrow and \downarrow runs. However, in a given target polarization state the beam polarization is reversed every accelerator pulse, hence, any motions or inefficiencies due to beam position fluctuations, will tend to be averaged away. Thus, N_{\uparrow} and N_{\downarrow} do not depend on the beam

polarization. Moreover, $P_T(\uparrow\uparrow) = P_T(\downarrow\downarrow)$, and $P_T(\uparrow\downarrow) = P_T(\downarrow\uparrow)$ to a very high precision.

The set of Eqs. (4.2) may be solved for A and C_m in various ways. We present an analytic solution in Appendix A. One can average the relations over the runs or apply standard methods of linear statistical analysis to obtain the least mean square solution for A and C_m . Both methods were used and agreed to $\pm 0.1\%$. The errors indicated by the statistical analysis were approximately $\pm 0.3\%$,

TABLE III. Wolfenstein parameters. The errors are statistical. There are also systematic normalization errors discussed in the text.

$P_{\perp}^2 [(\text{GeV}/c)^2]$	0.5 ^a	0.6	0.8	1.0
A	0.100 ± 0.003	0.091 ± 0.003	0.092 ± 0.003	0.144 ± 0.003
C_m	0.095 ± 0.004	0.107 ± 0.004	0.080 ± 0.004	0.057 ± 0.004
P	0.21 ± 0.05	0.06 ± 0.02	0.04 ± 0.03	0.09 ± 0.04
D_m	0.80 ± 0.10	0.85 ± 0.03	0.83 ± 0.04	0.76 ± 0.05
K_m	0.15 ± 0.06	0.13 ± 0.03	0.05 ± 0.04	0.04 ± 0.05
C_{3n}	0.16 ± 0.10	0.13 ± 0.05	0.12 ± 0.06	0.09 ± 0.08

^a The $P_{\perp}^2=0.5 (\text{GeV}/c)^2$ data are from Ref. 6; the errors there include an assumed 10% uncertainty in the analyzing power A_C .

while the pure "counting-rate" error was $\pm 0.1\%$.

It was necessary to make a small correction for inelastic contamination in $FB\bar{A}$. This contamination was studied during the Teflon runs, where we determined that $FB\bar{A}/N$ was $(3.9 \pm 0.2)\%$ of the normal rate, and that the measured $P_B(\uparrow) - P_B(\downarrow)$ asymmetry was about 40% of the normal elastic asymmetry. Apparently p -Teflon scattering has some spin dependence. This background required a relative correction to the measured A of about 2.5% and to C_{nn} of about 4%. Since A and C_{nn} are both approximately 10% the correction to A was about +0.25% and to C_{nn} about +0.4%. The uncertainty in this correction was less than $\pm 0.1\%$. We then used the values of A and C_{nn} to calculate the normalized four pure two-spin cross sections from Eqs. (2.10), (2.15):

$$\begin{aligned}\sigma(\uparrow\uparrow) &= [1 + 2A + C_{nn}], \\ \sigma(\uparrow\downarrow) &= [1 - 2A + C_{nn}], \\ \sigma(\downarrow\uparrow) &= \sigma(\downarrow\downarrow) = [1 - C_{nn}].\end{aligned}\quad (4.3)$$

The two-spin data analysis described above was done twice, independently. The results agreed within the errors and were averaged. The normalized two-spin cross sections and associated Wolfenstein parameters and their statistical errors are presented in Tables II and III.

B. Recoil polarization

For each of the four initial spin orientations in the p - p elastic experiment (beam, target) = $(ij) = \uparrow\uparrow, \uparrow\downarrow, \downarrow\uparrow, \text{ or } \downarrow\downarrow$, we used the measured asymmetry A_m^n and the A_C^n , D^n , and E^n obtained from the calibration runs to calculate the recoil-proton polarization $P_R^n(ij)$ for each of the 25 hodoscope channels (n) using Eq. (3.7). We then averaged P_R over the 25 channels weighting each channel according to the number of analyzed events

$$P_R(ij) = \frac{\sum_{n=1}^{25} [B_L^n(ij) + B_R^n(ij)] \frac{A_m^n(ij) - D^n}{A_C^n - A_m^n(ij) E^n}}{\sum_{n=1}^{25} [B_L^n(ij) + B_R^n(ij)]}.\quad (4.4)$$

With approximately 10^4 analyzed recoil polarimeter events at each P_\perp^2 the above relation gave a statistical error of about 5% in each $P_R(ij)$ at each P_\perp^2 . The values of the recoil polarization and their statistical errors are given in Table I.

If the beam and target had been both 100% polarized, we would immediately have the eight pure three-spin cross sections from the Eqs. (2.15) and (2.16) and the definition of P_R :

$$\begin{aligned}\sigma(ij \rightarrow 0\uparrow) &= \sigma(ij) [1 + P_R(ij)]/2, \\ \sigma(ij \rightarrow 0\downarrow) &= \sigma(ij) [1 - P_R(ij)]/2.\end{aligned}\quad (4.5)$$

C. Three-spin cross sections

In the actual experiment the beam and target were only partially polarized. To obtain the three-spin pure state normalized cross sections, Eq. (2.16), we can use the normalized versions of Eqs. (2.10) and (2.11):

$$N(ij) = 1 + [P_B(ij) + P_T(ij)]A + P_B(ij)P_T(ij)C_{nn},\quad (4.6)$$

$$\begin{aligned}P_R(ij)N(ij) &= P + P_B(ij)K_{nn} + P_T(ij)D_{nn} \\ &\quad + P_B(ij)P_T(ij)C_{3n}.\end{aligned}\quad (4.7)$$

The values of A and C_{nn} are known from the two-spin analysis, the $P_B(ij)$, $P_T(ij)$, and $P_R(ij)$ are measured in each of four (ij) states, allowing determination of the four Wolfenstein parameters P , K_{nn} , D_{nn} , and C_{3n} from Eqs. (4.6) and (4.7). The resulting cross sections are then obtained from Eq. (4.5) and the pure-state versions of (4.6) and (4.7). The values and errors can be found using standard statistical analysis.

Another derivation involving an explicit analytic matrix-inversion approach is presented in Appendix B. The results from the two methods were in agreement within the errors and averaged. These results, including the statistical errors, are presented in Tables II and III.

D. Error discussion

The statistical error in the beam polarization P_B was about $\pm 1\%$ for each 1-hour run. Each P_\perp^2 point had about 100 such runs so the statistical error in P_B was negligible. P_B also had a relative uncertainty of $\pm 6\%$ due to the uncertainty in the analyzing power of p - p elastic scattering at $P_\perp^2 = 0.5$ (GeV/c) 2 and 6 GeV/c. This uncertainty was the same for all points and is thus only a normalization uncertainty.

The target polarization P_T had a $\pm 4\%$ relative uncertainty coming from the temperature measurement used in calculating the thermal calibration constant in Eq. (3.3). There were also instabilities in the NMR system and slight variations in our NMR analysis method. We estimate that these together gave a 3% relative error. Adding these two errors in quadrature, the total relative error in P_T is $\pm 5\%$.

In the two-spin analysis procedure used, the effect of the polarization errors on A is primarily from P_B , giving a relative error of 6%, while the effect on C_{nn} is from the product $P_B P_T$ with relative error then of 8%. Since A and C_{nn} are about 0.1, the polarization error in A is about ± 0.006 absolute and in C_{nn} about ± 0.008 . These are predominantly normalization errors to be added to the

statistical errors given in Table III. Beam- and target-polarization errors are also to be added to the statistical errors of the two-spin cross-section ratios given in Table II: approximately ± 0.016 to the parallel cross-section ratios, ± 0.008 to the antiparallel.

The statistical errors in the three-spin cross sections were dominated by the $\pm 5\%$ statistical counting errors in the recoil-polarization measurements, giving errors of about ± 0.05 in the cross sections and Wolfenstein parameters, as shown in Tables II and III. In addition, there was a 6% relative normalization uncertainty in the determination of the recoil polarization, due to the uncertainty in the analyzing power of the 50-MeV polarimeter used in the recoil polarimeter calibration runs; this would produce relative 6% errors in the Wolfenstein parameters P , K_{nn} , D_{nn} , C_{3n} and would affect the cross sections, predominately through the parameter, D_{nn} . The statistical error in determining the recoil polarimeter parameters A_C , D , and E , during the calibration runs was $\pm \frac{1}{2}\%$ leaving the normalization uncertainty dominant. Also, as in the two-spin case, the effects of the beam and target relative polarization uncertainties, $\pm 6\%$ and $\pm 5\%$, would lead to equivalent relative errors in K_{nn} and D_{nn} , respectively, and to $\pm 8\%$ in C_{3n} . The cross sections again would be mostly affected through D_{nn} ; the sizes of these effects were usually smaller than the statistical errors.

The polarization parameter, P , involved in the parity and the time-reversal invariance tests, is very sensitive to misalignments, different inefficiencies, or different backgrounds in the two sides of the recoil polarimeter. A 1% polarimeter asymmetry with a polarimeter analyzing power $A_C = 0.5$, would lead to an error in P of ± 0.02 , comparable to the statistical errors shown in Table III. As discussed before, considerable care was taken to minimize these possible asymmetries, and we estimate their effects to be less than the statistical errors.

V. RESULTS AND DISCUSSION

A. Wolfenstein parameters

Table III contains a list of the Wolfenstein parameters measured in this experiment, obtained as discussed in the previous analysis section. The parameter D_{nn} is the correlation between the recoil polarization P_R and the target polarization P_T and equals 1 when there is no spin flip. Similarly, K_{nn} is the correlation between P_R and the beam polarization P_B and measures the spin transfer.

The parameters A , C_{nn} , K_{nn} , and D_{nn} are plotted in Fig. 8 along with other measurements at 6 GeV/

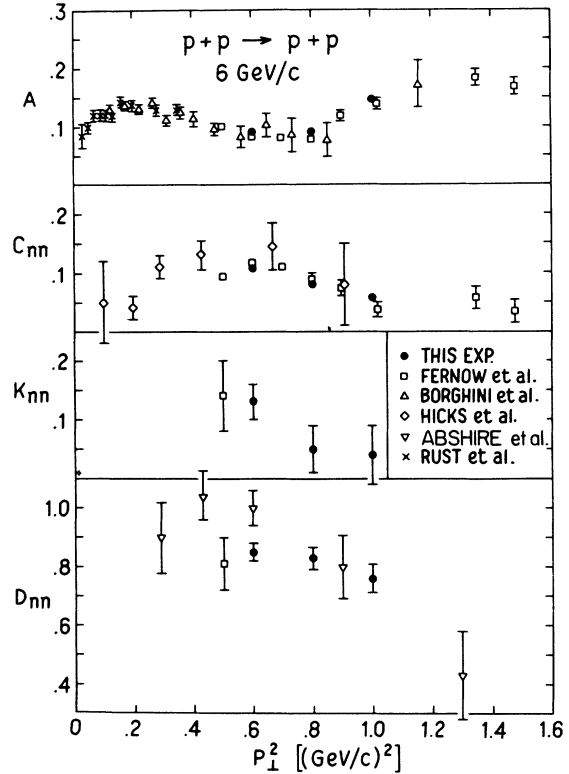


FIG. 8. The Wolfenstein parameters for p - p elastic scattering at 6 GeV/c are plotted against P_{\perp}^2 . The parameters A , C_{nn} , D_{nn} , K_{nn} are defined in Eqs. (2.20), (2.22), and (2.23). For some of the other experiments the bin sizes have been increased at large P_{\perp}^2 to improve the statistics. Some large-error points have been ignored. Recent results from Ref. 32 on low P_{\perp}^2 values of A are consistent with the plotted data.

$c^{2,5,6,19,20}$ Note that $D_{nn} \neq 1$ showing that spin flip does occur. Notice also that D_{nn} may be moving further from 1 at large P_{\perp}^2 , while K_{nn} moves towards 0. These two qualitative features should have a bearing on various strong-interaction models.²¹ Our values of D_{nn} are somewhat lower than those of Abshire *et al.*²⁰ at small P_{\perp}^2 . K_{nn} has not been measured by other groups. Our results on A and C_{nn} are in good agreement with earlier measurements, but have much better precision. Notice the maximum in C_{nn} around $P_{\perp}^2 = 0.6$ (GeV/c)². A has a minimum of $(8.4 \pm 0.3)\%$ at this P_{\perp}^2 , but is not equal to zero as at slightly higher energy.^{2,19,22}

B. Test of P and T

Consider the 16 pure four-spin cross-section ratios $\sigma(ij \rightarrow kl)$ (beam, target \rightarrow scattered, recoil). Each is the square of the amplitude $f(ij \rightarrow kl)$ for elastic scattering from a pure initial spin state (ij) to a pure final spin state (kl) . We measured

the eight pure three-spin cross sections, $\sigma(ij \rightarrow 0l)$, Eq. (2.16), each of which is the sum of two four-spin cross sections

$$\sigma(ij \rightarrow 0l) = \sigma(ij \rightarrow \uparrow l) + \sigma(ij \rightarrow \downarrow l). \quad (5.1)$$

There is an important theorem²³ which is valid for the elastic scattering of identical spin- $\frac{1}{2}$ particles when the spins are measured perpendicular to the scattering plane as in our experiment: If parity is conserved then all eight single-spin-flip trans-versity cross sections must equal zero. For each i, j , and l Eq. (5.1) contains one such single-flip $\sigma(ij \rightarrow kl)$ and either one double-flip or one nonflip term.

Now consider the four antiparallel three-spin cross sections that we measured:

$$\begin{aligned} \sigma(\uparrow\downarrow \rightarrow 0\uparrow) &= \sigma(\uparrow\downarrow \rightarrow \uparrow\uparrow) + \sigma(\uparrow\downarrow \rightarrow \downarrow\uparrow), \\ \sigma(\uparrow\uparrow \rightarrow 0\uparrow) &= \sigma(\uparrow\uparrow \rightarrow \uparrow\uparrow) + \sigma(\uparrow\uparrow \rightarrow \downarrow\uparrow), \\ \sigma(\uparrow\downarrow \rightarrow 0\downarrow) &= \sigma(\uparrow\downarrow \rightarrow \uparrow\downarrow) + \sigma(\uparrow\downarrow \rightarrow \downarrow\downarrow), \\ \sigma(\uparrow\uparrow \rightarrow 0\downarrow) &= \sigma(\uparrow\uparrow \rightarrow \uparrow\downarrow) + \sigma(\uparrow\uparrow \rightarrow \downarrow\downarrow). \end{aligned} \quad (5.2)$$

Parity implies that the four single-flip terms must be zero, and rotational invariance implies that for identical particles two equalities must hold:

$$\begin{aligned} \sigma(\uparrow\downarrow \rightarrow \uparrow\uparrow) &= \sigma(\uparrow\downarrow \rightarrow \downarrow\uparrow), \\ \sigma(\uparrow\uparrow \rightarrow \uparrow\uparrow) &= \sigma(\uparrow\uparrow \rightarrow \downarrow\uparrow). \end{aligned} \quad (5.3)$$

We now define and calculate the experimental quantity

$$\begin{aligned} \epsilon_P &= \sigma(\uparrow\downarrow \rightarrow 0\uparrow) - \sigma(\uparrow\uparrow \rightarrow 0\uparrow) \\ &= \sigma(\uparrow\downarrow \rightarrow \downarrow\uparrow) - \sigma(\uparrow\uparrow \rightarrow \downarrow\uparrow). \end{aligned} \quad (5.4)$$

This is listed in Table II and is equal to zero within errors at all P_{\perp}^2 . This implies that parity is conserved, or more properly, sets an upper limit on the difference between any parity-violating amplitudes.

We can test time-reversal invariance T by considering the two measured three-spin cross sections

$$\begin{aligned} \sigma(\uparrow\uparrow \rightarrow 0\uparrow) &= \sigma(\uparrow\uparrow \rightarrow \uparrow\uparrow) + \sigma(\uparrow\uparrow \rightarrow \downarrow\uparrow), \\ \sigma(\uparrow\downarrow \rightarrow 0\uparrow) &= \sigma(\uparrow\downarrow \rightarrow \uparrow\uparrow) + \sigma(\uparrow\downarrow \rightarrow \downarrow\uparrow). \end{aligned} \quad (5.5)$$

Parity invariance implies that the last two (single-flip) terms are zero, while T , and T alone, implies that

$$\sigma(\uparrow\uparrow \rightarrow \downarrow\uparrow) = \sigma(\uparrow\downarrow \rightarrow \downarrow\uparrow). \quad (5.6)$$

Since we have found no evidence for a parity violation, we define and calculate the experimental quantity

$$\begin{aligned} \epsilon_T &= \sigma(\uparrow\uparrow \rightarrow 0\uparrow) - \sigma(\uparrow\downarrow \rightarrow 0\uparrow) \\ &= \sigma(\uparrow\uparrow \rightarrow \uparrow\uparrow) - \sigma(\uparrow\downarrow \rightarrow \uparrow\uparrow). \end{aligned} \quad (5.7)$$

This is listed in Table II for each P_{\perp}^2 and is zero within the errors.

As indicated in Sec. IIB, an alternative way to test for P and T invariance is by using the Wolfenstein parameters listed in Table III. Parity invariance alone requires that $P = C_{3n}$, while time-reversal invariance alone requires that $A = P$. Again, the results appear in agreement with these relations within the errors.

We might summarize these conservation-law tests by saying that any P - or T -violating cross sections are consistent with being less than about 6% of $\langle d\sigma/dt \rangle$. It is especially interesting that there are no violations at our largest P_{\perp}^2 of 1.0 (GeV/c)² where these conservation laws had not been previously tested.

C. Pure spin cross sections

In Table II we list our measurements of $\sigma(ij \rightarrow 0l)$, the ratios of the three-spin cross sections to the spin average differential cross sections. This ratio is the quantity we measure with good precision.

We can now assume P and T invariance to reduce the 16 pure four-spin cross sections to the five independent pure spin cross sections corresponding to parallel (P) or antiparallel (A) initial spins, nonflip (nf) or double-flip (df) of the initial spins, and up (U) or down (D) for the parallel nonflip. These five independent $\sigma(ij \rightarrow kl)$ can be obtained from our eight measured three-spin cross sections using the relations:

$$\begin{aligned} \sigma(\uparrow\uparrow \rightarrow \uparrow\uparrow) &\equiv P_{df} = \frac{1}{2} [\sigma(\uparrow\uparrow \rightarrow 0\uparrow) + \sigma(\uparrow\downarrow \rightarrow 0\uparrow)], \\ \sigma(\uparrow\downarrow \rightarrow \uparrow\uparrow) &\equiv A_{nf} = \frac{1}{2} [\sigma(\uparrow\downarrow \rightarrow 0\uparrow) + \sigma(\uparrow\uparrow \rightarrow 0\uparrow)], \\ \sigma(\uparrow\downarrow \rightarrow \uparrow\downarrow) &\equiv A_{df} = \frac{1}{2} [\sigma(\uparrow\downarrow \rightarrow 0\downarrow) + \sigma(\uparrow\uparrow \rightarrow 0\downarrow)], \\ \sigma(\uparrow\uparrow \rightarrow \uparrow\downarrow) &\equiv U_{nf} = \sigma(\uparrow\uparrow \rightarrow 0\uparrow) + \frac{1}{2} [\sigma(\uparrow\uparrow \rightarrow 0\downarrow) - \sigma(\uparrow\downarrow \rightarrow 0\downarrow)], \\ \sigma(\uparrow\downarrow \rightarrow \uparrow\downarrow) &\equiv D_{nf} = \sigma(\uparrow\downarrow \rightarrow 0\downarrow) - \frac{1}{2} [\sigma(\uparrow\uparrow \rightarrow 0\downarrow) - \sigma(\uparrow\downarrow \rightarrow 0\downarrow)]. \end{aligned} \quad (5.8)$$

In the first three equations we reduce the experimental uncertainty by assuming P and T invariance and averaging. If the experimental data exactly conserved parity and time reversal U_{nf} and D_{nf} would be given by the first terms on the right-hand side. However, the data exhibit small differences which can either enhance or decrease U_{nf} and D_{nf} . We handle this by assigning half the difference to U_{nf} and half to D_{nf} . One could, of course, also determine these cross sections by redoing the statistical analysis using the additional P and T constraint relations.

The five independent $\sigma(ij \rightarrow kl)$ calculated using Eq. (5.8) are listed in Table II for each P_{\perp}^2 . The changes in the cross sections from the averaging procedure are minimal. We also list the $d\sigma/dt(ij \rightarrow kl)$ obtained by multiplying by the $\langle d\sigma/dt \rangle$ which is

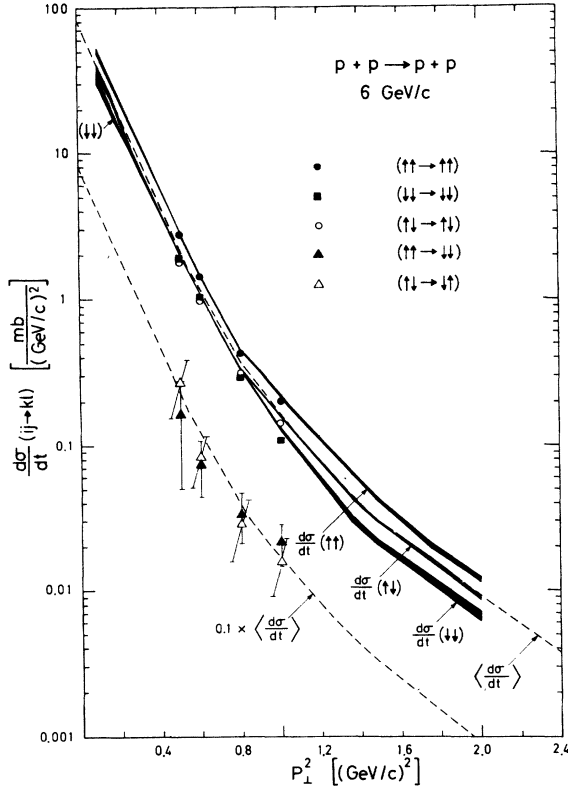


FIG. 9. Plot of the pure four-spin cross sections $d\sigma/dt(ij \rightarrow kl)$ for p - p elastic scattering at 6 GeV/c against P_{\perp}^2 . We also plotted the pure initial two-spin cross sections $d\sigma/dt(ij)$ as bands with widths corresponding to the errors. Also shown as dashed lines are the spin average cross section $\langle d\sigma/dt \rangle$ and 10% of $\langle d\sigma/dt \rangle$ for comparison with the double-flip cross sections. Notice that $P_{\perp}^2 = 2.40$ (GeV/c) 2 corresponds to 90° c.m. at 6 GeV/c.

taken from Ambats *et al.*¹⁷ at $P_{\perp}^2 < 1.0$ (GeV/c) 2 and from a compilation at large P_{\perp}^2 .²⁴ In Fig. 9 we plotted these five $d\sigma/dt(ij \rightarrow kl)$ against P_{\perp}^2 . The $\langle d\sigma/dt \rangle$ we used is plotted as a dashed line. We also plotted the three pure initial two-spin cross sections, Eq. (2.3), as bands whose widths correspond to the error at each P_{\perp}^2 . These errors are much smaller than those of the four-spin cross sections because the recoil polarization error does not contribute. For $P_{\perp}^2 \geq 0.5$ (GeV/c) 2 these $d\sigma/dt(ij)$ were obtained from Table II and our earlier publication,⁶ while for $P_{\perp}^2 < 0.5$ we combined the C_{nm} measurements of the ANL-Northwestern group⁵ with the A measurements of Borghini *et al.*²

D. Discussion

The most important feature of Fig. 9 is that the different spin states have quite unequal cross sections. The parallel-up cross sections $d\sigma/dt(\uparrow\uparrow \rightarrow \uparrow\uparrow)$

and $d\sigma/dt(\uparrow\uparrow)$ are sometimes twice as large as the parallel-down $d\sigma/dt(\downarrow\downarrow \rightarrow \downarrow\downarrow)$ and $d\sigma/dt(\downarrow\downarrow)$. The double-flip cross sections $d\sigma/dt(\uparrow\uparrow \rightarrow \downarrow\downarrow)$ and $d\sigma/dt(\downarrow\downarrow \rightarrow \uparrow\uparrow)$ are typically 10 times smaller than the nonflip. These large differences imply that spin must be considered in any serious model for strong interactions.²¹

Another very striking feature is the clear change in the spin dependence at about $P_{\perp}^2 = 0.8$ (GeV/c) 2 , where $d\sigma/dt$ has a break. In the "diffraction-peak" region below the break, the $d\sigma/dt(ij \rightarrow kl)$ are all parallel to each other, and $d\sigma/dt(\uparrow\uparrow \rightarrow \uparrow\uparrow)$ is about 50% larger than both $d\sigma/dt(\uparrow\uparrow \rightarrow \downarrow\downarrow)$ and $d\sigma/dt(\downarrow\downarrow \rightarrow \downarrow\downarrow)$. The cross sections have much more spin dependence in the region after the break where the $d\sigma/dt(ij)$ are again parallel, but now with a slope of $\sim \exp(-3.5 P_{\perp}^2)$. Here $d\sigma/dt(\uparrow\uparrow \rightarrow \uparrow\uparrow)$ is 100% larger than $d\sigma/dt(\downarrow\downarrow \rightarrow \downarrow\downarrow)$, while $d\sigma/dt(\uparrow\uparrow \rightarrow \downarrow\downarrow)$ is about halfway between.

There is some indication that the double-flip cross sections, especially $d\sigma/dt(\uparrow\uparrow \rightarrow \downarrow\downarrow)$, may become relatively larger after the break. This can be seen by comparison with the lower dashed curve which is 10% of $\langle d\sigma/dt \rangle$ or by studying $\sigma(\uparrow\uparrow \rightarrow \downarrow\downarrow)$ in Table II or D_{nm} in Fig. 8. This effect is a few standard deviations and thus is not certain; but it is an interesting possibility. It would be very significant if the double-flip cross section approached or exceeded the nonflip cross section at very large P_{\perp}^2 .

The break in $d\sigma/dt$ corresponds to the transition from the forward diffraction peak to the larger- P_{\perp}^2

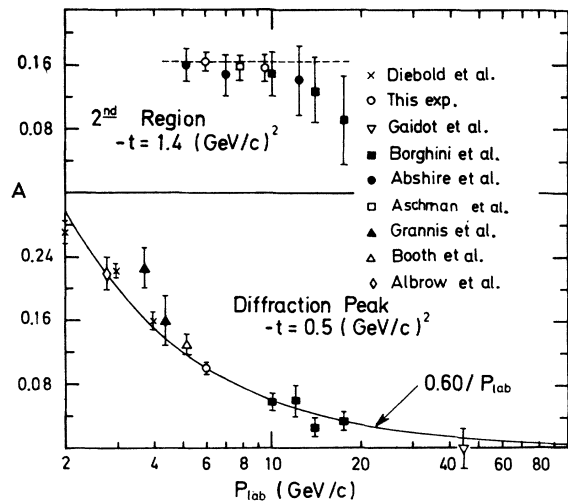


FIG. 10. Plot of the analyzing power A against incident lab momentum for p - p elastic scattering at fixed t . The lower graph shows A in the diffraction peak at $t = -0.5$ (GeV/c) 2 , while the upper shows A at $t = -1.4$ (GeV/c) 2 in the region after the break.

region. The large spin dependence in this second region may give important information about the nature of larger- P_{\perp}^2 elastic scattering. In Fig. 10 we compare our data^{6,25} with other energy measurements of A .^{1-3,19,22,26-28} It appears that the spin dependence disappears at high energy in the diffraction peak, but it may *not* disappear in the second region.

It is quite reasonable that the spin dependence in the diffraction peak should go to zero as $s \rightarrow \infty$. At high energy the peak becomes completely dominated by diffraction scattering, and one must average over the spin dependence of all inelastic channels contributing to diffraction through unitarity. Each channel may have a different spin dependence and they probably will tend to cancel. As shown in Fig. 10 the spin dependence disappears as $\sim 1/P_{\text{lab}}$ which is almost the same rate as the real part of the forward amplitude disappears. This is, in fact, further evidence that the "diffraction peak" is dominated by diffraction or shadow scattering. Similarly, the large- P_{\perp}^2 spin dependence not disappearing as $s \rightarrow \infty$ may indicate that this second region is not dominated by diffraction scattering, but is caused by some direct scattering mechanism. The amplitude in this larger- P_{\perp}^2 region must then be partly real. This may explain why the $\exp(-3.5P_{\perp}^2)$ term is disappearing at Fermilab²⁹ and CERN ISR³⁰ energies.

We plan to study this further by extending these measurements to higher energy and larger P_{\perp}^2 . It will be especially interesting to see if there is another change in the spin dependence as one enters the third region²⁴ of p - p elastic scattering at about $P_{\perp}^2 = 3.5$ (GeV/c)². If this third region is shadow scattering, then, like the diffraction peak, it should have little spin dependence at 12 GeV/c. If it is instead direct elastic scattering it may have a spin dependence similar to the second region. However, if the spin dependence is totally different, that may indicate that this third region is dominated by a second type of nondiffractive mechanism.

A brief paper summarizing this experiment has appeared earlier.³¹

ACKNOWLEDGMENTS

We are very grateful to the ZGS staff for the improved operation of the polarized beam. We would like to thank J. A. Bywater for his help in operating the PPT. We also thank Dr. S. W. Gray and Dr. E. F. Parker for their help in the early stages of the experiment and W. Dragoset, H. E. Haber, J. G. Toney, and A. L. Weil for their help in running. A.D.K. thanks the Niels Bohr Institute for their hospitality during a portion of the time this paper was being written.

APPENDIX A: ANALYTIC SOLUTION OF THE TWO-SPIN MATRIX EQUATION

Consider the four-event rate Eqs. (4.2):

$$\begin{aligned} N(\uparrow\uparrow) &= N_{\uparrow} \{ 1 + A [|P_B(\uparrow\uparrow)| + |P_T(\uparrow\uparrow)|] \\ &\quad + C_m |P_B(\uparrow\uparrow)| |P_T(\uparrow\uparrow)| \}, \\ N(\uparrow\downarrow) &= N_{\uparrow} \{ 1 + A [|P_B(\uparrow\downarrow)| - |P_T(\uparrow\downarrow)|] \\ &\quad - C_m |P_B(\uparrow\downarrow)| |P_T(\uparrow\downarrow)| \}, \\ N(\downarrow\uparrow) &= N_{\downarrow} \{ 1 + A [-|P_B(\downarrow\uparrow)| + |P_T(\downarrow\uparrow)|] \\ &\quad - C_m |P_B(\downarrow\uparrow)| |P_T(\downarrow\uparrow)| \}, \\ N(\downarrow\downarrow) &= N_{\downarrow} \{ 1 - A [|P_B(\downarrow\downarrow)| + |P_T(\downarrow\downarrow)|] \\ &\quad + C_m |P_B(\downarrow\downarrow)| |P_T(\downarrow\downarrow)| \}. \end{aligned} \quad (\text{A1})$$

For each target polarization we obtained the measured asymmetry defined by

$$A_m^+ \equiv \frac{N(\uparrow\uparrow) - N(\downarrow\uparrow)}{N(\uparrow\uparrow) + N(\downarrow\uparrow)}, \quad (\text{A2})$$

$$A_m^- \equiv \frac{N(\uparrow\downarrow) - N(\downarrow\downarrow)}{N(\uparrow\downarrow) + N(\downarrow\downarrow)}.$$

We next define the average beam and target polarizations and polarization differences for the target spin being \uparrow or \downarrow (+ or -) to be

$$\begin{aligned} P_B^+ &\equiv \frac{1}{2} [|P_B(\uparrow\uparrow)| + |P_B(\downarrow\uparrow)|], \\ \Delta P_B^+ &\equiv \frac{1}{2} [|P_B(\uparrow\uparrow)| - |P_B(\downarrow\uparrow)|], \\ P_T^+ &\equiv \frac{1}{2} [|P_T(\uparrow\uparrow)| + |P_T(\downarrow\uparrow)|], \quad \Delta P_T^+ = 0, \\ P_B^- &\equiv \frac{1}{2} [|P_B(\uparrow\downarrow)| + |P_B(\downarrow\downarrow)|], \\ \Delta P_B^- &\equiv \frac{1}{2} [|P_B(\uparrow\downarrow)| - |P_B(\downarrow\downarrow)|], \\ P_T^- &\equiv \frac{1}{2} [|P_T(\uparrow\downarrow)| + |P_T(\downarrow\downarrow)|], \quad \Delta P_T^- = 0. \end{aligned} \quad (\text{A3})$$

Then substituting Eq. (A2) into Eq. (A1) and simplifying, we obtain two equations of the form

$$1 = Aa^+ + C_m c^+, \quad (\text{A4})$$

$$1 = Aa^- + C_m c^-,$$

where the coefficients are given by

$$\begin{aligned} a^+ &\equiv P_B^+ / A_m^+ - (\Delta P_B^+ + P_T^+), \\ a^- &\equiv P_B^- / A_m^- - (\Delta P_B^- - P_T^-), \\ c^+ &\equiv P_T^+ (P_B^+ / A_m^+ - \Delta P_B^+), \\ c^- &\equiv -P_T^- (P_B^- / A_m^- - \Delta P_B^-). \end{aligned} \quad (\text{A5})$$

For each run with \uparrow target polarization we obtained values of a^+ and c^+ , while for each target \downarrow run we obtained values of a^- and c^- . For each pair of target \uparrow and \downarrow runs we then calculated A and C_m from the solution of Eq. (A4).

$$A = \frac{c^- - c^+}{c^- a^+ - c^+ a^-}, \quad (A6)$$

$$C_{nm} = \frac{a^- - a^+}{a^- c^+ - a^+ c^-}.$$

APPENDIX B: ANALYTIC DETERMINATION OF THE THREE-SPIN CROSS SECTIONS

To obtain the three-spin cross sections we calculate each of the normalized three-spin event rates $N(ij \rightarrow 0l)$ from the two-spin normalized event

rates $N(ij)$, Eq. (4.6), and the recoil polarizations $P_R(ij)$ for each initial spin state:

$$N(ij \rightarrow 0\uparrow) = N(ij) \left(\frac{1 + P_R(ij)}{2} \right), \quad (B1)$$

$$N(ij \rightarrow 0\downarrow) = N(ij) \left(\frac{1 - P_R(ij)}{2} \right).$$

Combining the above relations with Eqs. (2.6) and (2.7), one can show that these $N(ij \rightarrow 0l)$ are related to the normalized pure state three-spin cross sections $\sigma(ij \rightarrow 0l)$ by the matrix

$$\begin{bmatrix} N(\uparrow\uparrow \rightarrow 0l) \\ N(\uparrow\downarrow \rightarrow 0l) \\ N(\downarrow\uparrow \rightarrow 0l) \\ N(\downarrow\downarrow \rightarrow 0l) \end{bmatrix} = \begin{bmatrix} N_B^+ N_T^+ & N_B^+ (1 - N_T^+) & (1 - N_B^+) N_T^+ & (1 - N_B^+) (1 - N_T^+) \\ N_B^- (1 - N_T^-) & N_B^- N_T^- & (1 - N_B^-) (1 - N_T^-) & (1 - N_B^-) N_T^- \\ (1 - N_B^+) N_T^+ & (1 - N_B^+) (1 - N_T^+) & N_B^+ N_T^+ & N_B^+ (1 - N_T^+) \\ (1 - N_B^-) (1 - N_T^-) & (1 - N_B^-) N_T^- & N_B^- (1 - N_T^-) & N_B^- N_T^- \end{bmatrix} \begin{bmatrix} \sigma(\uparrow\uparrow \rightarrow 0l) \\ \sigma(\uparrow\downarrow \rightarrow 0l) \\ \sigma(\downarrow\uparrow \rightarrow 0l) \\ \sigma(\downarrow\downarrow \rightarrow 0l) \end{bmatrix}. \quad (B2)$$

The N_B^\pm and the N_T^\pm are the fraction of protons in each partially polarized initial spin state given by

$$N_B^+ = \frac{1}{2}(1 + P_B^+), \quad N_B^- = \frac{1}{2}(1 + P_B^-), \quad N_T^+ = \frac{1}{2}(1 + P_T^+), \quad N_T^- = \frac{1}{2}(1 + P_T^-), \quad (B3)$$

where P_B^\pm and P_T^\pm are defined in Appendix A. The ΔP terms, also defined in Appendix A, experimentally 0.01 or less, are assumed to be zero in this analysis. The four equations contained in the matrix equation each hold for the recoil spin up and down separately ($l = \uparrow$ or $l = \downarrow$).

To obtain the pure three-spin cross sections $\sigma(ij \rightarrow 0l)$ in terms of the $N(ij \rightarrow 0l)$, one must invert this matrix. The result is a matrix equation which holds for $l = \uparrow$ and $l = \downarrow$ separately.

$$\begin{bmatrix} \sigma(\uparrow\uparrow \rightarrow 0l) \\ \sigma(\uparrow\downarrow \rightarrow 0l) \\ \sigma(\downarrow\uparrow \rightarrow 0l) \\ \sigma(\downarrow\downarrow \rightarrow 0l) \end{bmatrix} = \begin{bmatrix} N_B^+ N_T^- & -N_B^- (1 - N_T^+) & -(1 - N_B^+) N_T^- & (1 - N_B^-) (1 - N_T^+) \\ -N_B^+ (1 - N_T^-) & N_B^- N_T^+ & (1 - N_B^+) (1 - N_T^-) & -(1 - N_B^-) N_T^+ \\ -(1 - N_B^+) N_T^- & (1 - N_B^-) (1 - N_T^+) & N_B^+ N_T^- & -N_B^- (1 - N_T^+) \\ (1 - N_B^+) (1 - N_T^-) & -(1 - N_B^-) N_T^+ & -N_B^+ (1 - N_T^-) & N_B^- N_T^+ \end{bmatrix} \begin{bmatrix} \frac{N(\uparrow\uparrow \rightarrow 0l)}{P_B^+ P_T} \\ \frac{N(\uparrow\downarrow \rightarrow 0l)}{P_B^- P_T} \\ \frac{N(\downarrow\uparrow \rightarrow 0l)}{P_B^+ P_T} \\ \frac{N(\downarrow\downarrow \rightarrow 0l)}{P_B^- P_T} \end{bmatrix}. \quad (B4)$$

The quantity $P_T \equiv \frac{1}{2}(P_T^+ + P_T^-)$. If one were able to always keep $P_T^+ = P_T^-$ and $P_B^+ = P_B^-$, then the superscripts could be eliminated and the matrix would be symmetric. In fact, at $P_1^2 = 1.0$ they were equal within 1%, but at other P_1^2 values they differed by up to 10%. For $P_1^2 = 0.6$ where they differed most the actual matrix was

$$\begin{bmatrix} 0.706 & -0.165 & -0.142 & 0.033 \\ -0.126 & 0.668 & 0.025 & -0.134 \\ -0.142 & 0.033 & 0.706 & -0.165 \\ 0.025 & -0.134 & -0.126 & 0.668 \end{bmatrix}.$$

Notice that because the beam and target were both highly polarized ($\sim 70\%$), the matrix is almost diagonal. For each P_1^2 we now use Eq. (B4) to calculate the eight different three-spin cross sections $\sigma(ij \rightarrow 0l)$ from the eight $N(ij \rightarrow 0l)$ obtained using Eq. (B1). The Wolfenstein parameters P , K_m , D_m , and C_m were then obtained using Eqs. (2.21)–(2.24).

*Work supported by U.S. Energy Research and Development Administration.

†Present address: Max Planck Institute für Physik, Munich, Germany.

‡Present address: Nordita DK 2100 Copenhagen, Denmark.

§Present address: Rice University, Houston, Texas 77001.

|| Present address: Argonne Universities Association, Argonne, Illinois 60439.

¹P. Grannis *et al.*, Phys. Rev. **148**, 1297 (1966).

²M. Borghini *et al.*, Phys. Lett. **24B**, 77 (1967); **31B**, 405 (1970); **36B**, 501 (1971); P. Bonamy *et al.*, Phys. Lett. **23**, 501 (1966); M. G. Albrow *et al.*, Nucl. Phys. **B23**, 445 (1970).

³N. E. Booth *et al.*, Phys. Rev. Lett. **21**, 651 (1968); **23**, 192 (1969); D. J. Sherden *et al.*, *ibid.* **25**, 898 (1970); J. H. Parry *et al.*, Phys. Rev. D **8**, 45 (1973).

⁴E. F. Parker *et al.*, Phys. Rev. Lett. **31**, 783 (1973); J. R. O'Fallon *et al.*, *ibid.* **32**, 77 (1974); W. de Boer *et al.*, *ibid.* **34**, 558 (1975); K. Abe *et al.*, Phys. Lett. **63B**, 239 (1976); H. E. Miettinen, thesis, Univ. of Michigan, 1975 (unpublished).

⁵G. Hicks *et al.*, Phys. Rev. D **12**, 2594 (1975); D. Miller *et al.*, Phys. Rev. Lett. **36**, 763 (1976); I. P. Auer *et al.*, *ibid.* **37**, 1727 (1976); **38**, 258 (1977).

⁶R. C. Fernow *et al.*, Phys. Lett. **52B**, 243 (1974).

⁷L. Wolfenstein, Annu. Rev. Nucl. Sci. **6**, 43 (1956); M. MacGregor, M. Moravcsik, and H. Stapp, *ibid.* **10**, 291 (1960); C. R. Schumacher and H. A. Bethe, Phys. Rev. **121**, 1534 (1961); S. Bilen'kii, L. Lapidus, and R. Ryndin, Zh. Eksp. Teor. Fiz. **49**, 1653 (1965) [Sov. Phys. JETP **22**, 1130 (1966)].

⁸L. Wolfenstein and J. Ashkin, Phys. Rev. **85**, 947 (1952).

⁹R. Fernow, Am. J. Phys. **44**, 560 (1976).

¹⁰T. K. Khoe, R. L. Kustom, R. L. Martin, E. F. Parker, C. W. Potts, L. G. Ratner, R. E. Timm, A. D. Krisch, J. B. Roberts, and J. R. O'Fallon, Part. Accel. **6**, 213 (1975).

¹¹R. M. Craig *et al.*, in *Proceedings of the Second International Symposium on Polarization Phenomena of Nucleons, Karlsruhe*, 1965, edited by P. Huber and H. Schopper (Birkhauser, Stuttgart, 1966), p. 322.

¹²M. Froissart and R. Stora, Nucl. Instrum. Methods **7**, 297 (1960).

¹³D. Cohen, Rev. Sci. Instrum. **33**, 161 (1962).

¹⁴E. F. Parker, in *High Energy Physics with Polarized Beams and Targets*, proceedings of the Argonne conference, 1976, edited by M. L. Marshak (AIP, New York, 1976), p. 382.

¹⁵J. Vermeulen, in *Proceedings of the Second International Conference on Polarized Targets*, edited by G. Shapiro (Univ. of California Press, Berkeley, 1971).

¹⁶J. Bywater, S. W. Gray, and R. C. Fernow, ANL Internal Report (unpublished). Also see H. E. T. Miettinen, thesis, University of Michigan, 1975 (unpublished) for further experimental details of the PPT, the polarized beam, and the F - B spectrometer.

¹⁷I. Ambats *et al.*, Phys. Rev. D **9**, 1179 (1974).

¹⁸D. Aebischer *et al.*, Nucl. Instrum. Methods **124**, 49 (1975) found $A = 0.526 \pm 0.022$ at 9° at 399 MeV for nearly elastic events (< 15 -MeV energy loss).

¹⁹G. W. Abshire *et al.*, Phys. Rev. Lett. **32**, 1261 (1974); D. R. Rust *et al.*, Phys. Lett. **58B**, 114 (1975).

²⁰G. W. Abshire *et al.*, Phys. Rev. D **12**, 3393 (1975).

²¹C. Bourrely, J. Soffer, and D. Wray, Nucl. Phys. **B77**, 386 (1974); **B91**, 33 (1975); J. Soffer and D. Wray, Phys. Lett. **43B**, 514 (1973); C. Bourrely and J. Soffer, Phys. Rev. D **12**, 2932 (1975); R. M. Delaney and J. L. Gammel, *ibid.* **12**, 1978 (1975); A. W. Hendry and G. W. Abshire, *ibid.* **10**, 3662 (1974); E. Gotsman and U. Maor, Nucl. Phys. **B96**, 167 (1975); C. Michael, Liverpool Report No. LTH5, 1975 (unpublished); E. Leader and D. Wray, Lett. Nuovo Cimento **16**, 289 (1976); E. Leader, and R. C. Slansky, Phys. Rev. **148**, 1491 (1966); R. J. N. Phillips, in *Proceedings of the International Conference on Polarized Targets and Ion Sources*, Saclay, France, 1966 (La Documentation Francais, Paris, 1967); E. Fermi, Nuovo Cimento **11**, 407 (1954); G. L. Kane and U. P. Sukhatme, Nucl. Phys. **B78**, 110 (1974); F. Halzen and G. H. Thomas, Phys. Rev. D **10** 344 (1974); T. T. Chou and C. N. Yang, Nucl. Phys. **B107**, 1 (1976); B. Kursunoglu, Phys. Rev. D **13**, 1538 (1976); L. Michel, in *High Energy Physics with Polarized Beams and Targets* (Ref. 14); M. G. Doncel, P. Minnaert, and L. Michel, CERN Report No. CERN Phys./747, 1974 (unpublished); Phys. Lett. **38B**, 42 (1972); N. Hoshizaki *et al.*, Prog. Theor. Phys. **45**, 1123 (1971); L. Puzikov, R. Ryndin, and I. Smorodinskii, Sov. Phys. JETP **5**, 489 (1967); M. Jacob and C. G. Wick, Ann. Phys. (N.Y.) **7**, 404 (1959); J. Raynal, Nucl. Phys. **28**, 220 (1961); R. J. N. Phillips, *ibid.* **43**, 413 (1963); N. H. Buttimore, Cavendish Laboratory report, 1971 (unpublished); J. Bystricky, F. Lehar, and P. Winternitz, Saclay report, 1976 (unpublished); E. L. Berger, Argonne Report No. ANL-HEP-PR 75-33, 1975 (unpublished); F. Halzen and C. Michael, Phys. Lett. **36B**, 367 (1971); L. Durand and F. Halzen, Nucl. Phys. **B104**, 317 (1976); R. D. Field and P. Stevens, Caltech Report No. CALT-68-534, 1976 (unpublished); F. E. Low, Phys. Rev. D **12**, 163 (1975); M. Moravcsik, review lecture, Troisieme Cycle de la Physique en Suisse Romande, 1976 (unpublished); P. Kolar, B. Z. Kopeliovich, and L. I. Lapidus, Czech. J. Phys. **B26**, 1294 (1976). See also Proceedings of the 1974 Argonne Summer Study on High Energy Physics with Polarized Beams, edited by J. B. Roberts [ANL Report No. ANL/HEP 75-02 (unpublished)], *High Energy Physics with Polarized Beams and Targets* (Ref. 14), and Proceedings of Symposium on Hadron Scattering, Liblice, Czechoslovakia, 1975 (unpublished).

²²D. G. Aschman *et al.*, Nucl. Phys. (to be published).

²³A. Bohr, Nucl. Phys. **10**, 486 (1959); A. Kotanski, Acta. Phys. Polon. **30**, 629 (1966).

²⁴A. D. Krisch, Phys. Rev. Lett. **19**, 1149 (1967).

²⁵We measured the p - p asymmetry parameter A at 9.5 GeV/ c during a short accelerator research run using the high-energy polarimeter with its unpolarized target. We obtained A from

$$A = \frac{1}{P_B} \left(\frac{L-R}{L+R} \right),$$

where P_B is the beam polarization. We measured L and R with good precision at both $P_1^2 = 1.2$ and 1.4 (GeV/ c)². The error is dominated by the uncertainty in P_B . We took P_B to be $(67 \pm 8)\%$ by measuring $P_B = (72 \pm 5)\%$ at 6 GeV and then noting that the measured

depolarization was less than 2% in jumping each of the three resonances between 6 and 9.5 GeV/c. The depolarization was measured by us and by the ZGS staff using a new high-statistics polarimeter built by CERN. The data for the two points at 9.5 GeV/c are

P_{\perp}^2 [(GeV/c) ²]	$\frac{(L-R)}{(L+R)}$	A
1.2	0.107 ± 0.011	0.160 ± 0.016
1.4	0.098 ± 0.011	0.146 ± 0.016

The lower limits on A are particularly safe because P_B at 9.5 GeV/c cannot be greater than at 6 GeV/c.

²⁶G. W. Abshire *et al.*, Phys. Rev. D 9, 555 (1974).

²⁷R. E. Diebold *et al.*, Phys. Rev. Lett. 35, 632 (1975).

²⁸A. Gaidot *et al.*, report presented at the European Physical Society International Conference on High Energy Physics, Palermo, 1975 (unpublished).

²⁹C. W. Akerlof *et al.*, Phys. Lett. 59B, 197 (1975).

³⁰N. Kwak *et al.*, Phys. Lett. 58B, 233 (1975).

³¹L. G. Ratner *et al.*, Phys. Rev. D 15, 604 (1977).

³²R. D. Klem *et al.*, Phys. Rev. D 15, 602 (1977).

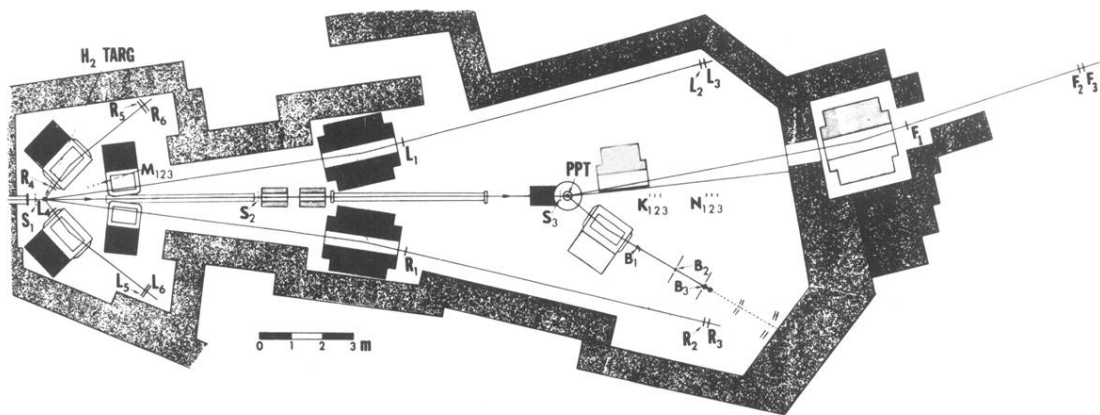


FIG. 1. Layout of the experiment. The polarized beam passes through the H_2 target, and its polarization is measured by comparing the number of elastic events seen in the L and R spectrometers of the polarimeter. The beam then scatters in the polarized proton target and the elastic events are counted by the FB spectrometer. The M , N , and K counters are monitors. The B polarimeter measures the spin of the recoil proton by measuring p -carbon scattering to the left and to the right.